Frontiers paper

The seismic mid-lithosphere discontinuity

Kate Selway [a],[*], Heather Ford [b], Peter Kelemen [a]

[a] *Lamont–Doherty Earth Observatory, Columbia University, Palisades, NY, USA*
[b] *Yale University, New Haven, CT, USA*

A B S T R A C T

Seismic S-wave receiver functions (SRF) are a uniquely powerful tool for imaging velocity discontinuities within the upper mantle. SRF data frequently contain negative phases at depths between ~80 and 100 km within the continental lithosphere, indicative of large and sharp velocity drops at these depths. In young, actively tectonic areas with thin lithosphere, this feature is generally interpreted as the lithosphere–asthenosphere boundary. However, in tectonically stable areas it occurs within the continental lithospheric mantle and has been termed the mid-lithosphere discontinuity (MLD). A significant velocity drop at such depths is unexpected and its cause is unknown. In this manuscript, we summarise the current observations and assess the main mechanisms that could produce such a feature. We find that changes in mantle iron content (Mg#) and elastically-accommodated grain-boundary sliding are unlikely to result in sufficiently large velocity decreases to produce an observable SRF response, while partial melt will generally only exist at greater depths within stable lithosphere. Radial and azimuthal seismic anisotropy are both capable of producing negative SRF phases. However, azimuthal anisotropy will not produce consistently negative phases independent of back-azimuth. Some geometries of radial anisotropy can produce consistent negative phases but such geometries are not observed universally and are hard to explain tectonically. Low-velocity minerals can cause sharp and large decreases in seismic velocity. Amphibole-rich layers are likely to form at MLD depths in metasomatised regions, making amphibole a possible cause for the MLD. However, some xenolith sections contain no amphibole, suggesting this may not be a universal explanation. A careful assessment of SRFs shows that the continental lithospheric mantle generally contains numerous positive and negative velocity discontinuities and is spatially heterogeneous. Long-period band-pass filtering can combine smaller features and may lead to the appearance of a larger and more coherent velocity decrease at the MLD than actually exists. We propose that many of the assessed mechanisms may be acting at different depths in different locations to produce numerous velocity discontinuities. The large MLD phase is likely to be commonly associated with amphibole but on current evidence there is no universal cause for the MLD.

© 2014 Elsevier B.V. All rights reserved.

1. Introduction

Where seismic shear-wave receiver function (SRF) studies (Farra and Vinnik, 2000; Zhou et al., 2000) have been carried out in the continents, they have consistently observed a decrease in seismic velocity at depths between ~60 and ~160 km and generally between ~80 and 100 km (Fig. 1) (e.g. Abt et al., 2010; Chen, 2009; Ford et al., 2010; Foster et al., 2014; Heit et al., 2007; Kumar et al., 2013; Savage and Silver, 2008; Sodoudi et al., 2013; Wittlinger and Farra, 2007; Wölbern et al., 2012). In some areas this seismic velocity decrease appears to be continuous between tectonically active areas and tectonically stable areas, such as across western USA (Foster et al., 2014) and across Australia (Ford et al., 2010). In tectonically active areas with thin lithosphere (~100 km thick), the velocity drop is generally interpreted as the lithosphere–asthenosphere boundary (LAB) (e.g. Ford et al., 2010; Foster et al., 2014; Heit et al., 2007). However, in stable continental and cratonic areas the lithosphere is ~150 to 300 km thick (Artemieva and Mooney, 2001; Carlson et al., 2005; Griffin et al., 2009; Jordan, 1978, 1988; Li et al., 2008; Schaeffer and Lebedev, 2013) and the cause for the velocity drop at ~80–100 km is not so clear. Indeed, it has been interpreted as a possible lithosphere–asthenosphere boundary (LAB) even in cratons (Rychert and Shearer, 2009), which is at odds with xenolith thermobarometry, heat flow and other geophysical data. It is therefore now widely agreed that this velocity reduction occurs at mid-lithospheric depths and it has been termed the mid-lithospheric discontinuity (MLD) (Abt et al., 2010).
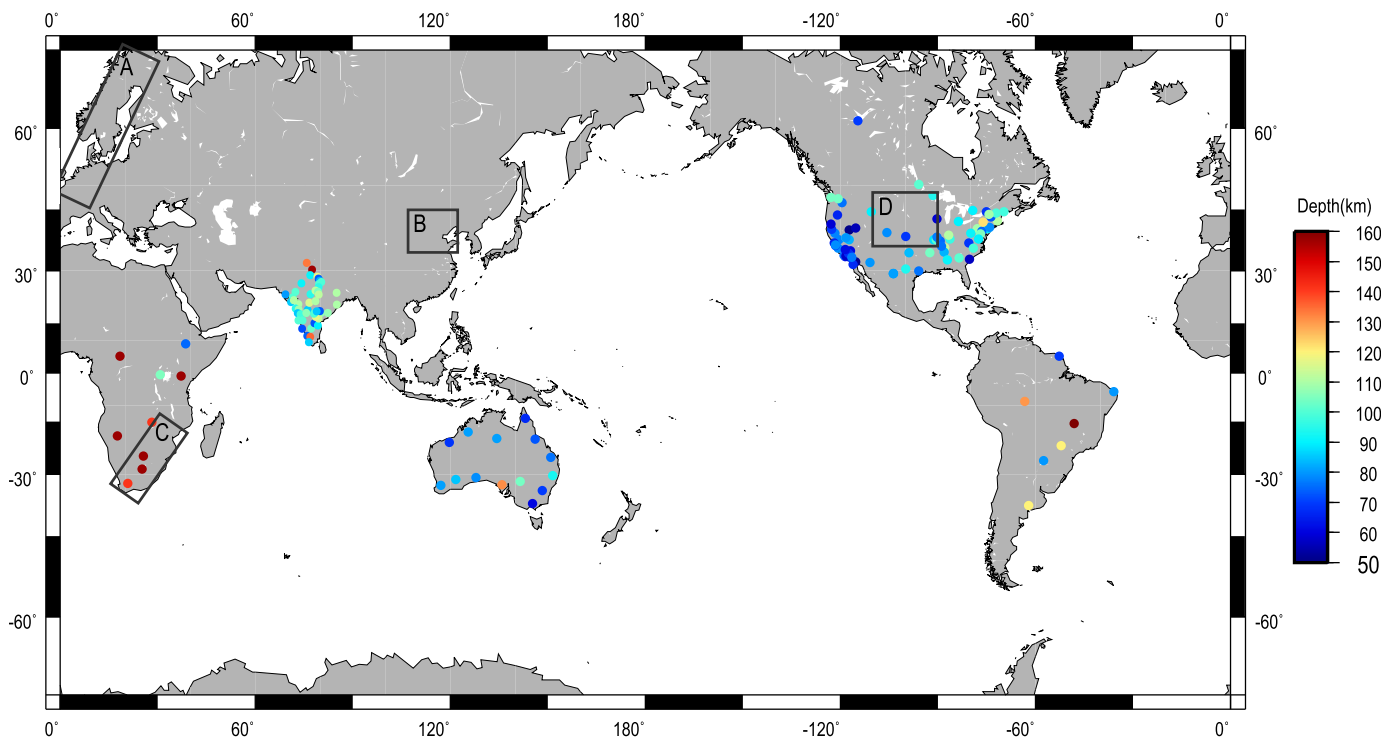
Fig. 1. Map of global observations of SRF data showing the depth to the largest negative phase beneath the Moho. Data are from North America (Abt et al., 2010; Rychert et al., 2007), Australia (Ford et al., 2010), South America (Heit et al., 2007), Africa (Hansen et al., 2009; Wölbern et al., 2012) and India (Kumar et al., 2013). Full coordinates are in the Supplementary Information. The mapped phases include those interpreted as the LAB (generally in actively deforming continental settings) or the MLD (generally in tectonically stable continental settings). Boxes A, B, C and D show the locations of dense station networks in Scandinavia (Kind et al., 2013), China (Chen, 2009, 2010), South Africa (Sodoudi et al., 2013) and western USA (Foster et al., 2014) for which SRF data have been published only as profiles. Although these cannot be displayed on this map, they show similar features to the single-station data, with large negative phases generally in the range of ∼80 to 100 km.

The presence of a sharp drop in velocity at mid-lithospheric depths in stable continents is unexpected and intriguing. Mantle xenoliths suggest that the compositions and geotherms of stable continents generally vary smoothly at mid-lithospheric depths (e.g. Carlson et al., 2005; Griffin et al., 2009) and provide no obvious cause for such a significant velocity drop. The apparent universality of the MLD in continental lithosphere (within the limits of current observations) makes a universal explanation for its cause desirable but mantle xenoliths and geophysical data show that the varied tectonic histories of cratons have resulted in heterogeneous lithospheric mantle (Rudnick et al., 1998; Selway, 2014; Silver, 1996). Moreover, the apparent contiguity of the velocity drop between tectonically active and stable regions raises the question of whether a single mechanism also applies to active areas although they have very different geotherms, compositions and tectonic histories than cratons. Therefore, while the cause for the MLD is not immediately clear from our current understanding of continental evolution, this very fact makes it an exciting new observation that has the potential to significantly develop our understanding. In this contribution, we will summarise and describe the SRF observations and assess their possible causative mechanisms in terms of seismic implications and geological feasibility.

2. Summary of seismic observations

Seismic body waves are either compressional 'P' waves, where particle motion occurs in the direction of energy propagation or shear 'S' waves where particle motion occurs perpendicular to the direction of propagation. When a P or S_V (vertically polarised S) wave encounters a sharp, isotropic velocity contrast, some of the transmitted energy is converted into the opposite wave type, i.e. P to S_V (Ps wave) and S_V to P (Sp wave) (Fig. 2). P waves travel faster than S waves so distinct primary (S or P) and converted (Sp
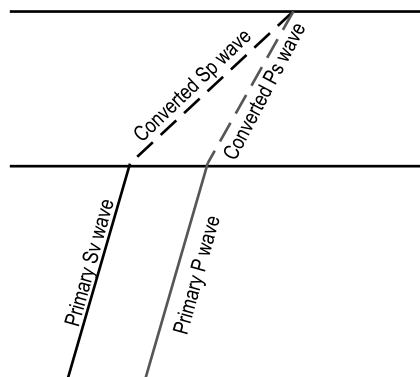

Fig. 2. When incident on a velocity discontinuity, some P wave energy will be converted to S wave energy (Ps wave) while some S-wave energy will be converted to P-wave (Sp wave) energy. Analysis of these converted waves at a seismic station (receiver) is referred to as the P-wave receiver function method (PRF) and the S-wave receiver function method (SRF) respectively.

or Ps) waves will be recorded at the Earth's surface. In the receiver function (RF) method, the depth to the velocity contrast is determined by measuring the difference in arrival times and estimating the subsurface velocity structure (Julià, 2007; Kind et al., 2012; Langston, 1979; Rychert et al., 2007; Yuan et al., 2006). Primary P waves with converted Ps waves are P-receiver functions (PRFs) while primary S waves with converted Sp waves are S-receiver functions (SRFs). RF data have significantly better depth resolution of velocity contrasts (±10 to 15 km) than surface wave tomography (±∼30 to 50 km) and body wave tomography (>50 km).

PRFs are of limited use for determining lithospheric mantle structure since crustal P-wave reverberations (multiples) arrive at similar times to the slower Ps waves from mantle velocity con-
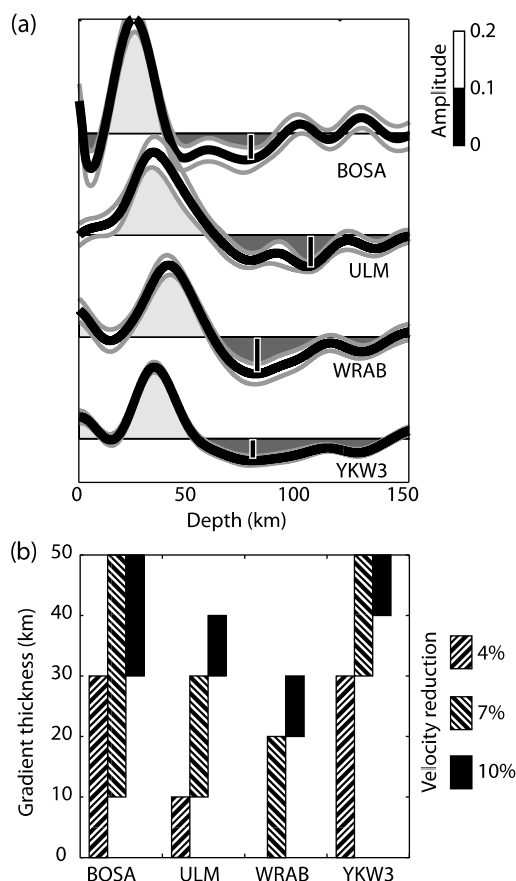
Fig. 3. (a) Calculated SRFs from stations WRAB (North Australia Craton) (Ford et al., 2010), ULM (Superior Craton) (Abt et al., 2010), YKW3 (Slave Craton) and BOSA (Kaapvaal Craton) (Wittlinger and Farra, 2007). Thick black line corresponds to the mean of the bootstrapped SRF and thin grey lines are the confidence intervals. Positive amplitudes are shown in pale grey while negative amplitudes are shown in dark grey. All four SRFs are scaled identically with an amplitude scale shown on the right. Black box with white outline in each SRF corresponds to the MLD phase being modelled in part (b). (b) Range of gradient thicknesses (within the confidence intervals) needed to match the amplitudes of the phases marked in (a) for assumed velocity reductions of 4%, 7% and 10%.

trasts (e.g. Rychert et al., 2007). In contrast, SRFs are ideal for determining mantle structure since the faster converted Sp waves arrive before the primary S waves and are therefore distinct from any crustal multiples. The SRF technique has only been used in any significant way since the year 2000 (Farra and Vinnik, 2000; Zhou et al., 2000) so the coverage of seismic stations with SRF data, while rapidly growing, does not yet extend to all geological regions. The negative phases observed in continental data at mid-lithospheric depths (Fig. 1) will be produced when seismic waves travel from a slower underlying layer to a faster overlying layer in a seismically isotropic setting.

The amplitude of an SRF phase is controlled by the magnitude and thickness of the velocity change, with higher amplitudes being produced by larger velocity contrasts and/or sharper velocity gradients. Where reported, velocity reductions associated with the MLD range from ∼3% in the western USA (Lekić and Fischer, 2014) and Kalahari Craton (Sodoudi et al., 2013) to over 10% in the Tanzanian Craton (Wölbern et al., 2012) (see Supplementary Information). Such magnitudes are comparable to or larger than velocity reductions observed at the continental LAB (Ford et al., 2010; Rychert et al., 2007; Sodoudi et al., 2013). Thicknesses of the velocity contrast are generally no more than 30 km to 40 km (Ford et al., 2010; Lekić and Fischer, 2014; Wölbern et al., 2012). We show four representative RF traces from cratonic regions in Fig. 3: station

WRAB (North Australia Craton, MLD 81 ± 14 km) (Ford et al., 2010), station ULM (Superior Craton, MLD 105 ± 12 km) (Abt et al., 2010), station YKW3 (Slave Craton, MLD 79 ± 18 km) and station BOSA (Kaapvaal Craton, MLD 78 ± 36 km) (Wittlinger and Farra, 2007), together with their calculated velocity contrasts and gradients, which fall within the published ranges. There is a limited range of phenomena that can physically account for such velocity reductions, all of which have been invoked by various authors to explain observed MLDs. They fall into three categories: (1) thermal phenomena, including the presence of partial melt and sub-solidus seismic relaxations in rocks, (2) compositional phenomena, including a reduction in mantle iron content and the presence of low-velocity minerals and (3) anisotropic phenomena, including changes in the geometry of radial and azimuthal seismic anisotropy. For the remainder of this paper, we will examine these proposed causes and assess them in terms of their physical plausibility and relationship to known geological processes.

3. Thermal cause

Temperature is the primary control on S-wave velocity in lithospheric mantle peridotites (Hughes and Cross, 1951) and the approximately consistent depth of the MLD across different cratons with similar geotherms suggests a thermal cause is possible. However, there are challenges to any purely thermal mechanism. Significant MLD topography is observed within cratons in some locations (e.g. eastern USA; Miller and Eaton, 2010) which suggests some non-thermal influence since cratonic geotherms are unlikely to have sharp lateral variations (Jaupart and Mareschal, 2011). Additionally, since temperature varies gradually and smoothly in cratonic lithospheric mantle, resulting variations in seismic wave velocities should also be gradual and smooth. Thermal causes are also unable to explain the contiguity between the on-craton and off-craton SRF phases. The two proposed mechanisms assessed below involve thermally-controlled phenomena that have a sharp onset, namely partial melting and elastically-accommodated grain-boundary sliding (GBS).

3.1. Option 1: partial melt

Seismic velocities are reduced in the presence of partial melt and several authors have suggested that a partial melt layer may be responsible for the MLD (Kumar et al., 2012; Thybo, 2006; Thybo and Perchuć, 1997). A comparison between experimental solidus temperatures (Dasgupta and Hirschmann, 2010; Green et al., 2010; Hirschmann, 2006; Till et al., 2012) and standard continental geotherms (e.g. Artemieva, 2009) shows that it is only possible for partial melt to exist at MLD depths if the lithospheric composition is rich in volatiles and/or if the MLD is deeper than average (>150 km) (Fig. 4). The only experimental solidus that crosses cratonic geotherms at the depth of most MLD observations is for an undepleted, chlorite-rich, water over-saturated composition (Till et al., 2012) that is unrepresentative of depleted and volatile-poor cratons (e.g. Griffin et al., 2009). One of the deepest interpreted MLDs, at ∼150 km depth, is at station BOSA in the Kaapvaal Craton, South Africa (Hansen et al., 2009; Wittlinger and Farra, 2007) (Fig. 2) and is therefore one of the most likely MLDs to be caused by partial melt. Since partial melt is electrically conductive compared to crystalline rock, we tested the feasibility of a melt layer by comparing magnetotelluric (MT) data from nearby station KAP025 (Moorkamp et al., 2010) with forward models of Kaapvaal lithosphere containing a partial melt layer at 150 km depth. Electrical conductivity of the melt was calculated assuming a basaltic composition with water contents 3 to 6 wt% at 1150 °C (Ni et al., 2011), while crystalline rock conductivity was
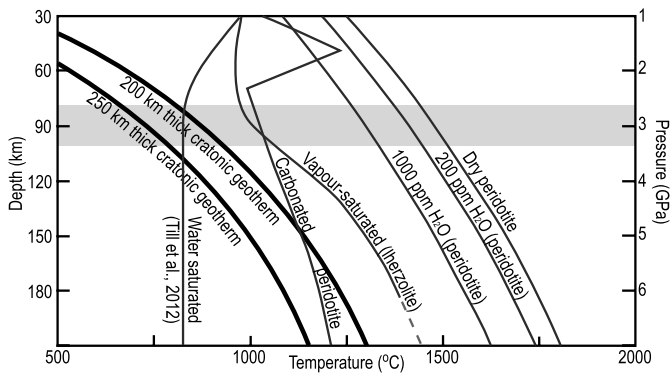
Fig. 4. Experimental solidus temperatures (Dasgupta, 2013; Dasgupta and Hirschmann, 2010; Green et al., 2010; Hirschmann, 2006) and standard continental geotherms (e.g. Artemieva, 2009). Grey shaded area represents the depth range of most MLD observations, which are at least 150 °C below any solidus temperatures. MLDs at depths >150 km could be explained by partial melt in a volatile-rich setting.

taken from 1D MT inversions (Supplemental Information). This calculation is conservative since carbonatite melt is more likely to be present and has higher conductivity than basaltic melt (Sifré et al., 2014). The melt proportion necessary to produce the MLD is likely to be at least 2% (e.g. Hammond and Humphreys, 2000). All models produce a characteristic peak in the MT phase that is not observed in station data (Fig. 5), suggesting that a partial melt layer is not responsible for the deep MLD at BOSA. Such a peak is a general feature of MT data responding to a conductive layer within a more resistive background and is not commonly observed in cratonic MT data (Selway, 2014). Additionally, our calculations (Fig. 3) and those of Sodoudi et al. (2013) do not image an MLD at such depths at BOSA. More generally, even assuming that the Till et al. (2012) solidus applies to cratonic upper mantle worldwide, there is no obvious reason why melt, migrating by porous flow in peridotite, should accumulate to significant porosities at 80–100 km depth. While new observations could discover deep MLDs caused by partial melt, current evidence suggests that shallower MLDs and the deep MLD at BOSA are not caused by partial melt.

3.2. Option 2: elastically accommodated grain-boundary sliding

The seismic velocity of mineral aggregates decreases with increasing temperature as their behaviour transitions from elastic to anelastic. Raj and Ashby (1971) showed that there is a point in this transition where applied stresses produce elastically-accommodated movement on grain boundaries due to their low effective viscosities, termed elastically-accommodated grain-boundary sliding (GBS). This theory predicts a frequency and temperature-dependent peak in seismic attenuation (and an associated potentially sharp decrease in seismic velocity) that is superimposed on the more gradual, background velocity decrease (Fig. 6). Recent experimental data have begun to observe this attenuation peak (e.g. Faul and Jackson, 2005; Jackson and Faul, 2010; Jackson et al., 2014; Morris and Jackson, 2009; Sundberg and Cooper, 2010) and suggest that at seismic frequencies it should occur at a temperature of ∼1000 °C in olivine. This led Karato (2012) to suggest that GBS could cause the MLD although most MLD occurrences occur between ∼700 and 900 °C (Fig. 4). This is an appealing suggestion since GBS appears to be a ubiquitous phenomenon and therefore does not require different cratons to have similar geological histories.

To test whether GBS could produce the MLD, lithospheric mantle velocity profiles based on a Kaapvaal Craton geotherm (Artemieva, 2009) with average 'Archon' composition (Griffin et al., 2009) incorporating a GBS velocity drop were constructed and re-
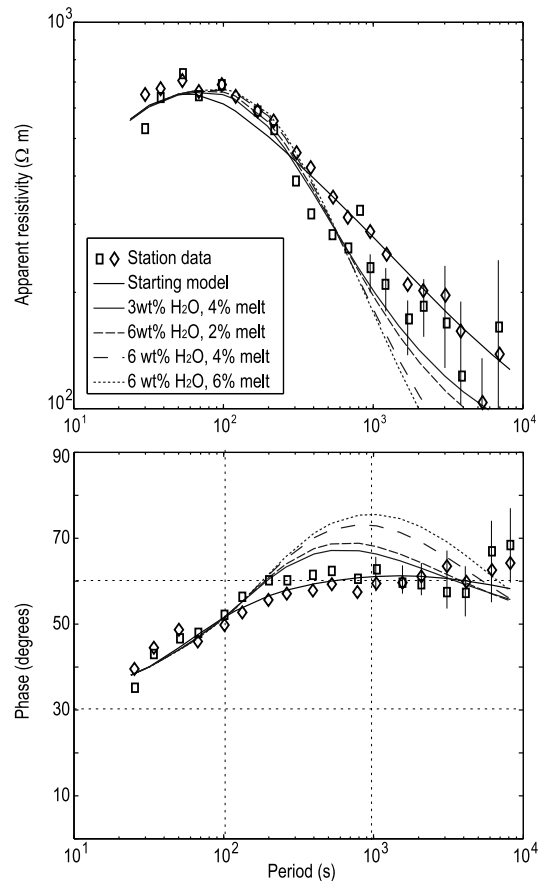

Fig. 5. Comparison between station data (Moorkamp et al., 2010) and the forward modelled response of a layer of between 2% and 5% basaltic partial melt containing between 3 wt% and 6 wt% water at 150 km depth at station KAP025 in the Kaapvaal Craton. The presence of melt produces a characteristic peak in MT phase that is not observed in the station data.
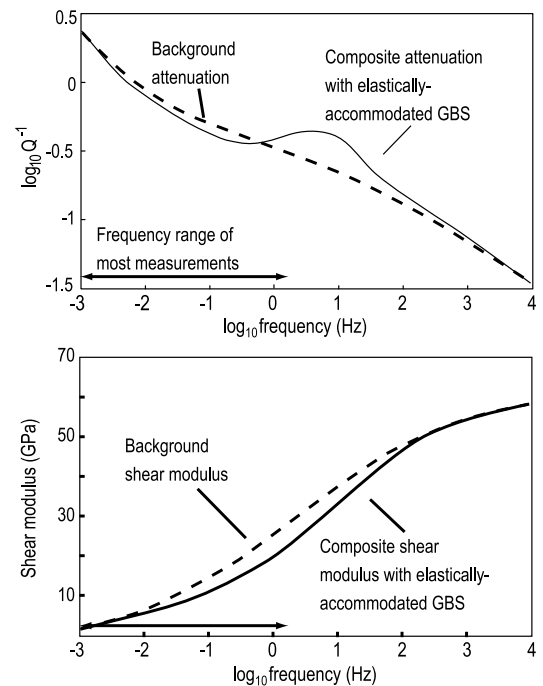

Fig. 6. Elastically accommodated grain-boundary sliding causes a frequency-dependent peak in seismic attenuation. Shaded area represents the frequency band over which current experimental data extend, showing that the peak width is currently poorly constrained.
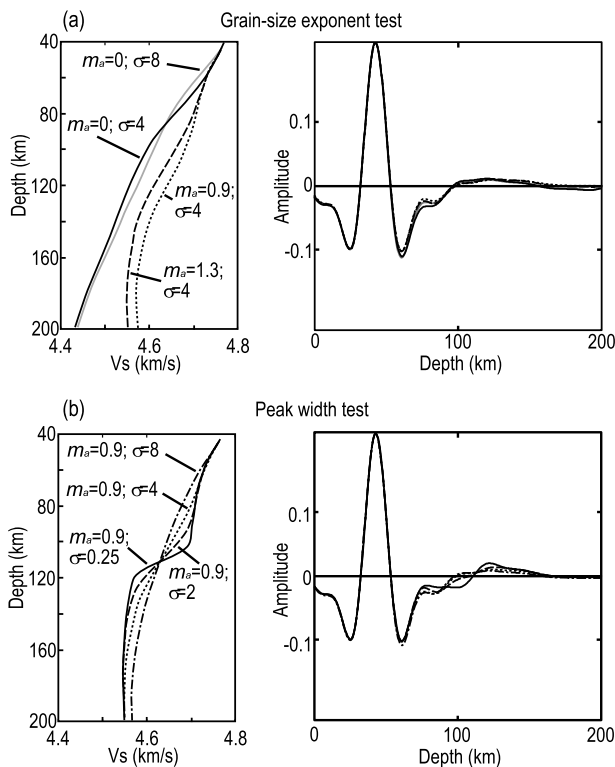
Fig. 7. S-wave velocity–depth sections and resulting forward modelled SRFs for typical 200 km thick lithosphere incorporating the effects of elastically accommodated grain-boundary sliding, using formulations in Jackson and Faul (2010). (a) Shows the variations resulting from changing the grain-size exponent between 0, 0.9 and 1.3 while (b) shows the variations resulting from changing the peak width between 0.25 and 8. GBS calculations were made at 0.5 Hz and the SRFs were band-width filtered at 0.05–0.5 Hz. No combination of parameters produces a negative phase large enough to be interpreted as the MLD.

sulting receiver functions were forward modelled. The GBS velocity profiles were based on Jackson and Faul (2010) (Supplementary Information). Some key parameters in the GBS formulation remain poorly constrained. For instance, only the high-frequency edge of the peak has been observed so the peak width is poorly determined (Fig. 6). Experiments have all been carried out on aggregates with homogeneous grain-sizes but peak magnitude is likely to decrease by 50% if even two different grain sizes are present (Lee and Morris, 2010). Experimentally, larger grain-sizes exhibit a smaller attenuation peak, but some theoretical analyses assert that GBS should be independent of grain-size (e.g. Olugboji et al., 2013; Sundberg and Cooper, 2010). Therefore, in producing the velocity–depth sections, grain-size exponents $m_a = 0$ (no grain-size sensitivity), $m_a = 0.9$ (preferred model in Jackson and Faul, 2010) and $m_a = 1.3$ (preferred model in Jackson et al., 2014) and peak widths $0.25 \leq \sigma \leq 8$ (preferred model in Jackson and Faul, 2010 has $\sigma = 4$) were tested. A typical cratonic lithospheric mantle grain size of 5 mm (e.g. Ave Lallemant et al., 1980) was assumed.

Velocity–depth sections show that the magnitude of velocity reduction is much larger if there is no grain-size dependence but the gradient of the velocity drop is only sharp if a peak width of 0.25 is assumed, which is significantly below current fits to experimental data (Fig. 7). The shear-wave velocity profiles were used to compute SRFs using a propagator matrix method (Ford et al., 2010; Keith and Crampin, 1977) and a simultaneous frequency domain deconvolution (e.g. Bostock, 1999) following the methodology outlined in Abt et al. (2010) using a bandpass filter of 0.05 to 0.5 Hz. Resulting SRF traces have either no or negligible negative phases (Fig. 7). The largest negative phase is produced by a peak width of 0.25 but its magnitude is significantly smaller than MLD ob-

servations (Fig. 3). Therefore, on the basis of current experimental results, it does not seem plausible that GBS is responsible for the MLD. This is especially true since current experimental results are for pure, homogeneous samples and the GBS peak magnitude will decrease and its width will increase for substances with heterogeneous grain-sizes and compositions. For this analysis to change, further experimental results would have to meet the following criteria: (1) the peak width must be ∼0.25, (2) grain-size sensitivity must be ∼0, (3) the existence of heterogeneous grain-sizes (or grain-boundary viscosities) must not reduce the magnitude of the peak significantly.

4. Compositional cause

After temperature, major element chemistry (i.e. the ratio between Fe and Mg, Mg# = 100 Mg/(Mg + Fe)) is the main cause of velocity anomalies in lithospheric mantle peridotite (e.g. Schutt and Lesher, 2006). A younger, juvenile underplate with an increased Mg# has been interpreted to be associated with the MLD in North America (Yuan and Romanowicz, 2010). Alternatively, large velocity decreases can be produced by low-velocity minerals, especially hydrous minerals produced through metasomatism (e.g. Connolly and Kerrick, 2002; Hacker et al., 2003). A layer of hydrous minerals has been interpreted as the cause for the MLD in several places including the Kalahari Craton (Savage and Silver, 2008; Sodoudi et al., 2013) and the Tanzanian Craton and East Africa Rift (Wölbern et al., 2012). A challenge for such compositional models is to reconcile them with models of craton formation and evolution. Models of craton formation, either through stacking of subducted slabs or plume accretion, are unlikely to produce substantial changes in S-wave velocity at mid-lithospheric depths (Aulbach et al., 2007; Lee, 2006). Even if such features were produced during craton formation, different cratons have subsequently had very different tectonic evolutions (e.g. Carlson et al., 2005; Griffin et al., 2009). Any compositional model for MLD as a global feature must address how that particular composition can exist in all stable continental lithosphere despite different patterns of tectonism, melting, depletion and re-fertilisation.

4.1. Option 1: change in Mg#

Experimental data show that a change in Mg# of more than 5 is needed to produce a velocity reduction of ∼2% (Priestley and McKenzie, 2006; Schutt and Lesher, 2006), which is smaller than the velocity reduction for most reported MLD observations. Mg# measurements from mantle xenoliths do not show evidence for such extreme variations in Mg# (Griffin et al., 2009), even in the Slave Craton which is distinctive and unrepresentative among cratons for having strongly layered lithosphere (Griffin et al., 2004; Kopylova and Russell, 2000). For instance, an MLD at ∼72 km depth at station YKW3 in the northern Slave Craton (Ford, 2013) is close to a step decrease in Mg# (Kopylova and Russell, 2000) but this decrease is only from Mg# ∼93 to Mg# ∼92, corresponding to a velocity reduction of <1% at 3 GPa (Schutt and Lesher, 2006). In North America a juvenile underplate associated with a decrease in Mg# and a change in anisotropy has been interpreted to be the cause of the MLD (Yuan and Romanowicz, 2010) but there is no evidence of a correlation between Mg# or anisotropy and MLD depth (Fig. 8). As in most continental lithosphere sections, the steep gradient in Mg# occurs at depths greater than the MLD, near the base of the lithosphere. For example, Kaapvaal Craton Group 1 xenolith Mg# are ∼92 to 93 from ∼90 to 160 km depth, followed by a sharp decrease to ∼89 at ∼180 km depth (Griffin et al., 2009; Carlson et al., 2005). More broadly, Re–Os mantle xenolith ages from North America, the Pilbara Craton and the Kaapvaal Craton show that ancient lithospheric mantle exists both below and above
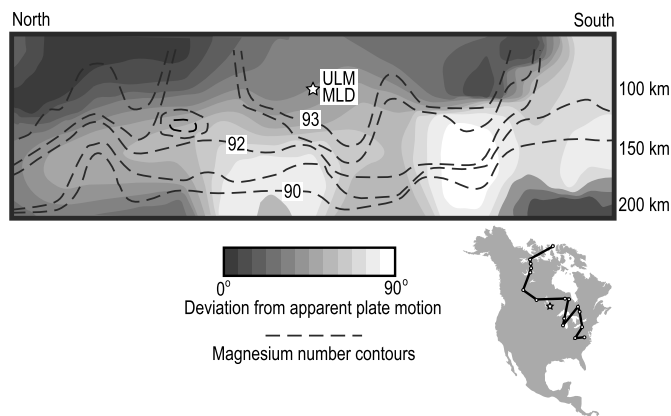
Fig. 8. Comparison between anisotropy direction (grey shading) (Yuan and Romanowicz, 2010), Mg# (dashed contours) (Griffin et al., 2004) and MLD depth at station ULM (Abt et al., 2010) in North America. Yuan and Romanowicz (2010) proposed that the North American MLD is caused by a juvenile lithospheric underplate that is associated with both a change in anisotropy (grey shading) and a sharp decrease in Mg#. However, there are no sharp decreases in Mg# at MLD depths and no clear relationship between anisotropy and Mg#.

MLD depths with no evidence for significantly juvenile underplates or voluminous metasomatism that could cause a large change in Mg# (Graham et al., 1999; Griffin et al., 2004; Richardson et al., 2001). Mantle xenoliths therefore do not support a change in Mg# as the MLD cause.

4.2. Option 2: hydrous minerals

Hydrous mantle minerals have substantially slower seismic velocities than the nominally anhydrous mantle minerals such as olivine, pyroxene and garnet (e.g. Hacker et al., 2003) and could therefore produce the velocity drops necessary to explain MLD observations. Although not compositionally dominant within the lithospheric mantle, hydrous minerals are commonly observed within mantle xenolith sections (e.g. Best, 1974b; Griffin et al., 1984; Konzett et al., 2013) and are generally interpreted to have been produced through metasomatism.

For any hydrous mineral to cause the MLD, it must exist in a significant volume only at depths below the MLD; if it were to extend throughout the lithosphere it would not cause a discrete velocity decrease at the MLD. Amphibole is the only mineral likely to fulfil this criterion. Amphibole is stable in peridotite bulk compositions at a pressure of ≤ 3 GPa over a broad temperature and compositional range (Fig. 9) (Wyllie, 1987). Thus, the maximum pressure of amphibole stability corresponds to the depth of most MLD observations (Fig. 1). Ascending hydrous melt and/or aqueous fluids, in equilibrium with mantle peridotite, might first crystallise amphibole at ~3 GPa, forming a "crystallisation front" which is likely to extend over only a small depth interval due to the fast reaction kinetics in the mantle. In contrast, phlogopite, the other common hydrous mantle mineral, has much higher maximum pressure and temperature of stability (Fig. 9) (e.g. Frost, 2006; Sweeney et al., 1993). The temperature independence of the amphibole stability field at 3 GPa suggests that amphibole could explain not only the MLD within cratons but also the velocity decrease at similar depths interpreted as the LAB in some active continental settings (Fig. 1).

To test whether amphibole could produce the MLD observations, we calculated the volume of amphibole that could be produced through the interaction between a bulk rock composition of either pyrolite (Ringwood, 1966) or abyssal peridotite (Dick, 1989) and various compositions of aqueous fluid (pure water and the island arc basalt fluid source of Ayers et al., 1997) or melt (Grand Canyon basanite lavas '1' and '6' from Best, 1970) to produce four
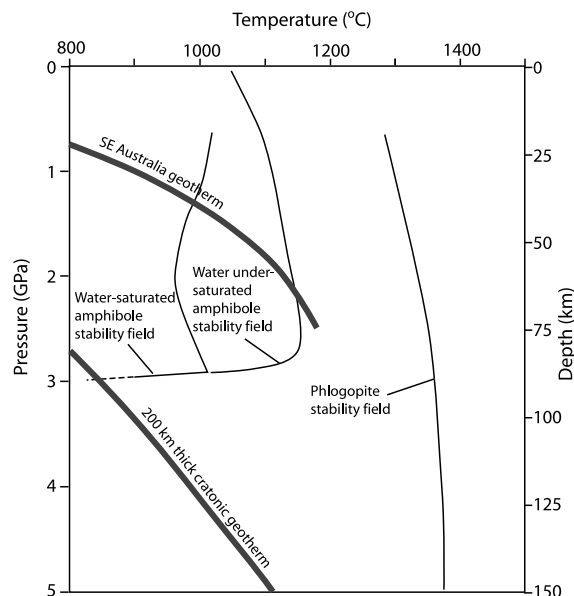

Fig. 9. Stability fields of water-saturated and water-under saturated amphibole and of phlogopite (Frost, 2006) with a typical geotherm for 200 km thick, cratonic lithosphere (Artemieva, 2009) and the tectonically active eastern Australian geotherm (O'Reilly and Griffin, 1985). Amphibole will crystallise at ~3 GPa for most settings except those with very high geotherms and/or very hydrous compositions. Phlogopite is representative of other hydrous minerals that will be stable over a broader depth range.

different compositions of amphibole (pure amphibole compositions $(Na, K)Ca_2((Mg, Fe)_{4.5}(Cr, Al)_{0.5})(Si_{6.5}(Cr, Al)_{1.5})O_{22}(OH)_2$ (hornblende) and $(Na, K)Ca_2((Mg, Fe)_4(Cr, Al)(Si_6(Cr, Al)_2)O_{22}(OH)_2$ (pargasite) and Grand Canyon amphiboles '2' and '10' from Best, 1970) (Fig. 10). We assumed that the entire mixture solidified to produce olivine + pyroxenes + spinel + amphibole, with the exception of any excess water. In the case where pure water interacted with an abyssal peridotite rock to produce pure pargasite, only 1.5% pargasite is produced. However, the interaction between pure water and pyrolite produces 18% amphibole. All interactions involving either Ayers fluid or Grand Canyon melts produce amphibole contents >22%. Testing showed that small changes to the specific composition of the fluid, reactant and amphibole do not significantly affect these results. The highest amphibole contents (>50%) were produced when Grand Canyon basanite melt compositions were used to produce Grand Canyon amphiboles. From this analysis, velocity–depth profiles incorporating amphibole were constructed. Kaapvaal Craton lithospheric mantle mineralogy, Mg# (Griffin et al., 2009, HP database) and geotherm (Artemieva, 2009) were used as base models. From the analysis described above, we took an average of 25% amphibole from 75 km to 95 km depth and added 1% phlogopite through the whole depth range. An additional model was produced that drew upon the volume of hydrous minerals measured in the Kaapvaal Craton by Waters and Erlank (1988), which reach a maximum of ~11% at ~80 km depth. Seismic velocities were calculated using the macro of Hacker and Abers (2004) and SRFs were forward modelled. Both models result in velocity decreases of >5% and produce negative SRF phases that fall within the bootstrap confidence intervals of typical real SRF data (Supplementary Information) and could be interpreted as the MLD (Fig. 11).

Since it is possible to produce volumes of amphibole sufficient to produce the MLD, the remaining challenge for this hypothesis is whether amphibole exists throughout all parts of cratonic lithosphere where an MLD is observed. Xenolith sections commonly show zones of metasomatism (Griffin et al., 2009), which could result from fluids or melts ascending from upwelling mantle into the overlying lithosphere (e.g. Chesley et al., 1999;
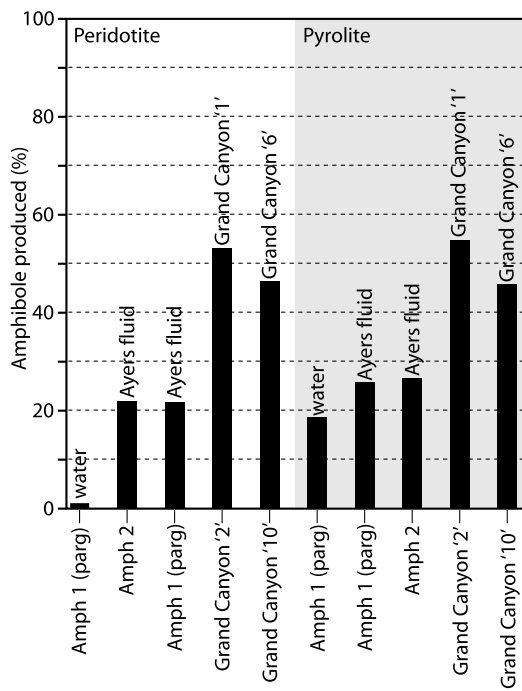
Fig. 10. Models of the likely proportion of amphibole produced through various fluid/melt and rock interactions. Each column represents the percentage of amphibole produced when a fluid or melt (named at the top of each column: pure water, Ayers fluid, Ayers et al., 1997, or the melt compositions represented by Grand Canyon basanite lavas '1' and '6' of Best, 1970) interacts with either abyssal peridotite or pyrolite to produce amphiboles of four different compositions (named at the base of each column: pure amphibole 1 (pargasite), pure amphibole 2 ($NaCa_2(Mg_{4.5}Al_{0.5})(Si_{6.5}Al_{1.5})O_{22}(OH)_2$) and Grand Canyon amphibole compositions '2' and '10' of Best, 1970). Most interactions produce amphibole proportions of at least 20%.

Kelemen et al., 1998). If these fluids/melts ascend to 3 GPa, they are likely to crystallise amphibole. However, xenolith data suggest that this may not occur ubiquitously (Table 1). Some regions contain significant volumes of amphibole, including the Gawler Craton (southern Australia), eastern Australia, western USA and the Kaapvaal Craton. In the western USA and some eastern Australian localities there is excellent agreement between amphibole observations and MLD depth but in the Kaapvaal Craton and south-eastern Australia (Victoria) there is a significant difference between the depth at which amphiboles are observed in xenoliths and the depth of the MLD (Table 1). Very large velocity decreases of 12% and 24% beneath the Tanzanian Craton and East Africa Rift respectively may not be related to amphibole but could be caused by abundant, metasomatic phlogopite and pyroxenite (Wölbern et al., 2012). On the other hand, abundant amphibole and phlogopite have not been reported from the Udachnaya pipes in the Siberian Craton or the bulk of the Slave Craton, both of which are well sampled by xenoliths that cover depths at which amphibole would be stable. Seismic data from the Slave Craton show an MLD at ∼70 to 80 km depth. There are currently no SRF data for the Siberian Craton but such data would comprise an excellent further test of this model.

Rudnick et al. (1998) argued that the bulk cratonic mantle was unlikely to be as metasomatised as many xenolith suites since cratonic geotherms and low surface heat flows were only possible if the average cratonic K_2O content (which they estimated to be 0.03 wt%) is much lower than that of average cratonic xenoliths (0.148 wt%). The hydrous mineral model for the MLD implies substantial precipitation of K-bearing amphibole has only occurred in a narrow zone at ∼3 GPa whereas Rudnick et al. (1998) assumed a constant concentration of K_2O throughout the cratonic lithospheric mantle. To assess the heat flow implications of the
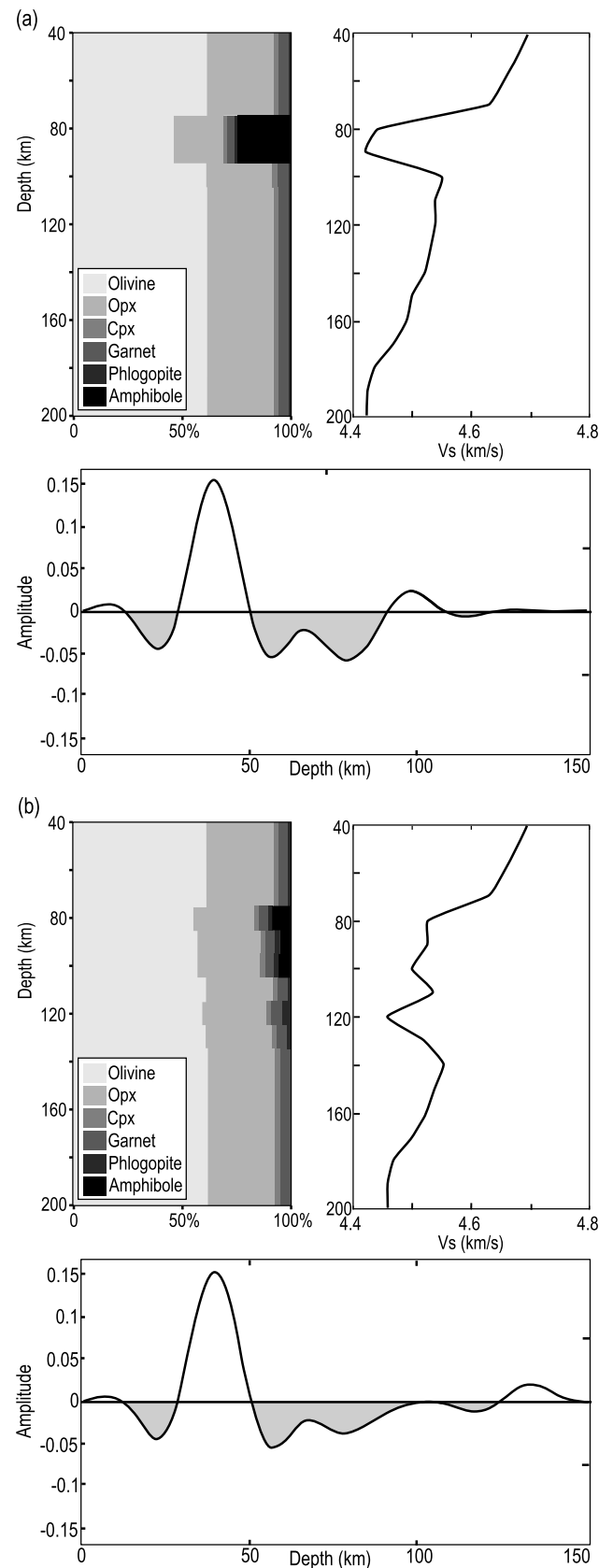
Fig. 11. Modal compositions, S-wave velocity–depth sections and resulting forward modelled SRFs for (a) a mantle based on Kaapvaal Craton geotherm and average craton composition with 25% amphibole from 75 km to 95 km depth and 1% phlogopite throughout and (b) as above, but with volumes of hydrous minerals taken from the Kaapvaal Craton (Waters and Erlank, 1988). Both models produce observable phases that could be interpreted as the MLD and contain realistic SRF complexity.

Table 1

Table stating whether xenolith studies in various locations have reported amphibole presence (Y = yes, N = no) and at what depth, along with the depth of any proximal negative phases from SRF data. Text in italics refers to the depth ranges of analysed xenoliths where no amphibole is reported. Amphibole percentage refers to the amount of amphibole within the xenoliths except where noted. Numbers in parentheses refer to references as follows: (1) Ford et al. (2010); (2) Abt et al. (2010); (3) Ford et al. (2010); (4) Sodoudi et al. (2013); (5) Hansen et al. (2009); (6) Ferguson and Sheraton (1979); (7) Wass and Rogers (1980); (8) Griffin et al. (1984); (9) Griffin and O'Reilly (1986); (10) Powell et al. (2004); (11) Handler et al. (2005); (12) Edwards et al. (1992); (13) Downes et al. (2007); (14) Luguet et al. (2009); (15) Tappe et al. (2008); (16) Meyer et al. (1994); (17) Vicker (1997); (18) Best (1974a); (19) Wilshire et al. (1980); (20) Griffin et al. (1999); (21) Kopylova and Russell (2000); (22) Kopylova et al. (1999); (23) Kopylova and Caro (2004); (24) Carbno and Canil (2002); (25) Pearson et al. (1995); (26) Boyd et al. (1997); (27) Ionov et al. (2006); (28) Hawkesworth et al. (1990); (29) Konzett et al. (2000); (30) Waters and Erlank (1988); (31) van Achterbergh et al. (2001).

Continent	Location	Amphibole present?	Depth/*xenolith depths*	Amphibole percentage	Proximal negative SRF phase depth	Seismic station and reference
Australia	Gawler Craton, Pt Augusta	Y (6)	–	Up to 10%	131 km	BBOO (1)
	Eastern Australia, Jugiong	Y (6)	60–75 km	–	70 km	YNG (1)
	Eastern Australia, Kiama	Y (7)	–	Up to 90%	70 km	YNG (1)
	South-eastern Australia, SW Vic	Y (8, 9, 10)	40.5 km	Up to 32.5%	61 km	TOO (1)
	North-eastern Australia, NE Qld	N (11)			73 km	CTAO (1)
	Western Australia, Kimberley	N[a] (12, 13)			81 km[b]	FITZ (1)
	Western Australia, Argyle	N (14)	*>90 km*		81 km[b]	FITZ (1)
North America	Labrador	Y (15)	–	–	–	
	Superior Craton	N[a] (16, 17)	*>105 km*		101 km[b]	ULM (2)
	Western USA, Grand Canyon	Y (18)	65 km		61 km	GSC (2)
	Western USA, Deadman Lake, CA	Y (19)	–	30% of xenoliths contain amphibole	70 km	WDC (2)
	Slave Craton, Lac de Gras	N (20)	*>90 km*	–	–	
	Slave Craton, Jericho	N/rare grains (21, 22)	*>60 km*	–	79 km[b]	YKW3 (3)
	SE Slave Craton	N[a] (23)	–	–	–	
	SW Slave Craton	Y (24)	–	–	71 km[b]	JERN (3)
Eurasia	Siberian Craton, Udachnaya	N[a] (25)	*>93 km*	–	–	
	Siberian Craton, Udachnaya	N[a] (26)	*>75 km*	–	–	
	Siberian Craton, Tok	Y (27)	–	–	–	
Africa	Kaapvaal Craton, Kimberley	Y (28, 29, 30)	*<120 km*, 111 km	<10% of xenoliths contain amphibole[c]. 11% hydrous minerals at <825 °C	80 km[b] and 157 km[b]	(4) and (5)
	Botswana, Letlhakane	N (31)	*>135 km*		160 km	(5)

[a] No amphibole present but other hydrous minerals are present.
[b] Interpreted as an MLD.
[c] From an assessment of >600 thin sections (Hawkesworth et al., 1990).

proposed amphibole layer, we compiled xenolith data from the Kaapvaal Craton, eastern Australia and western USA, giving average amphibole K_2O contents of 4.82 wt% (Konzett et al., 2013; Sweeney et al., 1993), 0.995 wt% (Griffin et al., 1984) and 1.16 wt% (Best, 1974a, 1974b; Wilshire et al., 1980) respectively. Using heat flow equations and average MORB K:U:Th ratios given in Jaupart and Mareschal (2011), a 20 km thick section containing 15% amphibole with a Kaapvaal composition would indeed produce a large contribution to surface heat flow of 7.06 mW/m². However, amphiboles with eastern Australian and western USA compositions would produce surface heat flow contributions of only 1.47 and 1.7 mW/m² respectively, which are insignificant in comparison to average heat flows in Archean cratons (41 mW/m², $s.d. = 11$) and Early Proterozoic cratons (46 mW/m², $s.d. = 15$) (Nyblade and Pollack, 1993). Therefore, while the high K amphibole in Kaapvaal Craton xenoliths are potentially unrepresentative of material that is abundant in the bulk cratonic mantle, the lower K concentration in mantle amphibole from other regions indicates that a 20 km thick section of amphibole with such compositions could be present in many or most cratons, and cannot be ruled out on the basis of surface heat flow.

5. Anisotropic cause

Variations in the geometry of seismic anisotropy can produce conversions in both SRFs and PRFs (e.g. Crampin, 1984; Levin and Park, 1997). Azimuthally anisotropic layers related to lithospheric stacking during craton formation have been interpreted to cause observed PRF conversions in the Slave Craton (Bostock, 1998;

Mercier et al., 2008; Snyder, 2008) while Rychert and Shearer (2009) suggested that a negative PRF phase at mid-lithospheric depths within the cratons could be caused by a change from stronger to weaker radial anisotropy with depth. Variations in azimuthal anisotropy have been observed at MLD depths in central USA (Wirth and Long, 2014). If such features are globally extensive, it is possible that the MLD could be caused by changes in the geometry of seismic anisotropy within the mantle. However, the dependence of converted phases on anisotropy geometry and the variation of anisotropy with tectonic history pose significant challenges to this hypothesis.

An olivine-dominated rock with a stress-induced fabric and lattice-preferred orientation (LPO) of olivine grains will have a seismic fast direction aligned with the rock fabric (Karato et al., 2008). Lithospheric mantle anisotropy is therefore 'frozen in' by previous tectonothermal events. In general, incident S and P waves can produce converted Sp and Ps phases when incident on a radially anisotropic (vertical axis of symmetry) or azimuthally anisotropic (horizontal axis of symmetry) layer (Fig. 12). For azimuthally anisotropic layers, the polarity of the conversion is controlled by the orientation of the fast direction of anisotropy compared to the direction of wave propagation and the back-azimuth (Fig. 12) (Frederiksen and Bostock, 2000), resulting in a 180° back-azimuth periodicity in the polarity of the converted phase (Frederiksen and Bostock, 2000; Levin and Park, 1997; Savage, 1998; Sodoudi et al., 2013) and the unlikelihood of azimuthal anisotropy producing consistently negative phases.

In an isotropic Earth, coupling occurs between P and S_V waves while the P–S_V remains decoupled from S_H. In an anisotropic
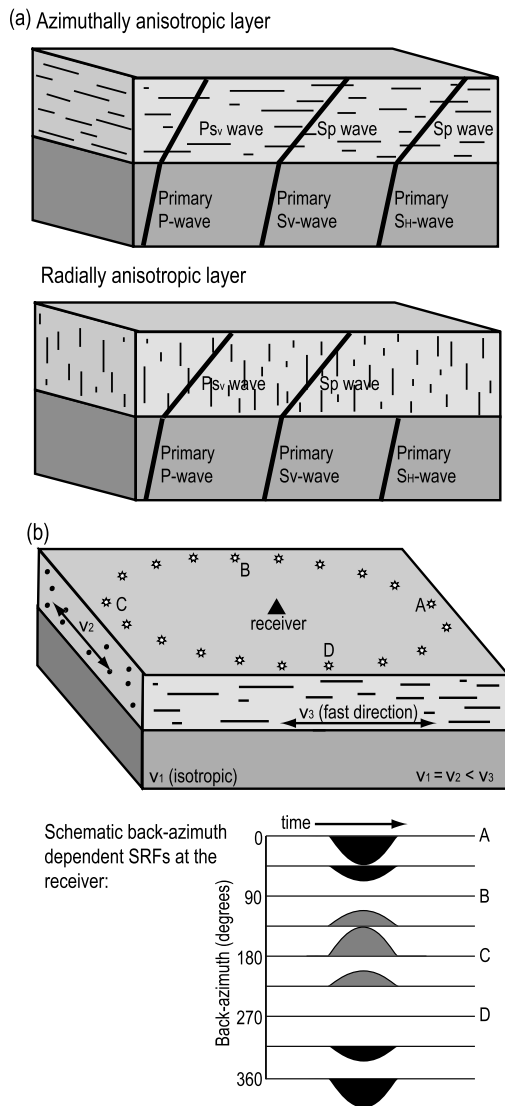
Fig. 12. Schematic of RF responses at anisotropic layers. (a) Wave conversions at azimuthally and radially anisotropic layers. (b) SRF conversions produced when an azimuthally anisotropic layer (S-wave velocities $v_2 = v_1$ and $v_3 > v_1$) overlies an isotropic layer (S-wave velocity v_1) have a 180° back-azimuth dependence. Triangle denotes a seismic receiver and stars denote earthquake locations at different back-azimuths. Schematic SRFs for back-azimuth directions varying between points A, B, C and D vary between positive, negative and no conversions.

Earth, coupling can occur between P, S_V, and S_H, which has been utilised in P–S_H RF analysis to investigate azimuthal anisotropy (e.g. Levin and Park, 1997). Theoretically, SRFs should also be capable of utilising coupling between P–S_V–S_H to image azimuthally anisotropic structure. An important caveat is that the form of the Sp conversion depends on the polarity (S_V or S_H) of the primary wave (Bourguinon, 2009; Frederiksen and Bostock, 2000). Preliminary modelling shows that the ratio of incident S_V and S_H energy and the choice of deconvolution component (radial-S_V or transverse-S_H) affects (1) the polarity of the more prominent converted phase (positive or negative) and (2) the back-azimuth at which polarity changes from positive to negative. Importantly, the ratio of incident S_V and S_H energy is dependent on the focal mechanism of the earthquake, as well as the location of the earthquake relative to the station. The complexities of Sp conversions at azimuthally anisotropic layers warrant further investigation and may be a powerful tool for determining mantle anisotropy. However, these complexities mean that even if a simple, azimuthally anisotropic layer exists in the mantle, the SRF response to that

layer would include an array of both positive and negative conversions and therefore such a feature cannot be the global cause for the MLD.

Radial anisotropy, as suggested by Rychert and Shearer (2009), appears to be a simpler explanation for a consistently negative Sp phase since a vertical axis of symmetry will yield Sp conversions that are independent of back-azimuth. S_H waves do not produce Sp conversions at boundaries of radially anisotropic layers, so there is no additional complexity related to the ratio of primary S_V and S_H energy. Ford (2013) modelled synthetic mantle structures consisting of an underlying isotropic layer with an overlying radially anisotropic layer with a vertical axis of symmetry and showed that it is possible to produce consistent negative SRF phases for certain anisotropy geometries.

Tectonically, the case for a consistent geometry of anisotropy throughout all stable continental lithosphere is difficult to make. Since strain during major tectonic events can re-orient LPO (e.g. Jung et al., 2006) it is not enough to invoke a mechanism for forming a uniform anisotropy in cratonic mantle during its formation; one must also argue that this anisotropy survives all later tectonic events or that the disparate tectonic events experienced by different cratons all produce the same anisotropy. Most continental studies show significant spatial variations in azimuthal anisotropy which can often be related directly to tectonic events (Fouch and Rondenay, 2006). Mantle azimuthal anisotropy from surface wave phase velocities in the Kaapvaal Craton varies consistently with tectonic region (Adam and Lebedev, 2012), as does seismic anisotropy in the uppermost 150 to 200 km of cratonic central and western Australia (Debayle and Kennett, 2000; Simons and van der Hilst, 2002, 2003). In cratonic North America, Yuan and Romanowicz (2010) presented evidence for a two-layer anisotropic structure but updated results in Yuan et al. (2011) show that, while a mid-lithospheric change in anisotropy is often observed, anisotropy is complex and related to tectonic environment. Wirth and Long (2014) show that SRF data in central USA require a complex, two-layer anisotropic structure with specific directions of azimuthal anisotropy in each layer. The interpreted remnants of fossil subducted slabs in the Slave Craton (Bostock, 1998) have been invoked by many authors as an analogue for converted phases elsewhere (e.g. Kind et al., 2013; Levin and Park, 2000; Saul et al., 2000) but, as described in the previous section, xenoliths from the Slave Craton show a unique, compositionally layered structure that is unrepresentative of global cratonic xenolith suites (Kopylova and Caro, 2004), making it unlikely that the Slave Craton exhibits globally representative seismic structure. Although there are fewer studies of radial anisotropy than azimuthal anisotropy, their implications for the MLD are similar. Radial anisotropy with a fast horizontal axis is likely to be caused by sub-horizontal flow and may be associated with azimuthal anisotropy (e.g. Lebedev et al., 2009). Radial anisotropy in lithospheric mantle across North America (Marone et al., 2007; Nettles and Dziewoński, 2008; Yuan et al., 2011), Australia (Debayle and Kennett, 2000; Fichtner et al., 2010), Africa (Saltzer, 2002; Sebai et al., 2006) and globally (Lebedev et al., 2009; Nettles and Dziewoński, 2008) generally shows faster horizontal wavespeeds than vertical wavespeeds ($V_{SV} < V_{SH}$) with a magnitude that decreases with depth from the Moho. However, the magnitude of the anisotropy is generally <4% (Lebedev et al., 2009; Nettles and Dziewoński, 2008), which is too small to account for the MLD phase. Additionally, detailed studies in North America show significant lateral variations not only in the strength but also in the polarity of radial anisotropy (Nettles and Dziewoński, 2008; Yuan et al., 2011). The contrasting radial anisotropy patterns in the oceanic mantle, which do show a homogeneous, sharp and large change at ~100 km depth (Nettles and Dziewoński, 2008), could produce consistent negative SRF phases.

Globally, azimuthal and radial anisotropy data show complex and spatially variable behaviour, including from regions with observed MLDs. Since the SRF response to azimuthal anisotropy is also complex and spatially variable, it is not reasonable for azimuthal anisotropy to be a global cause for the MLD, although it may produce negative phases in SRFs in some locations. Since the SRF response to radial anisotropy is less complex, radial anisotropy anomalies may produce more negative SRF phases. However, observed variations in the polarities of radial anisotropy anomalies and the absence of anomalies in many areas show that this also cannot be a global explanation for the MLD. Amphibole has a moderately large single crystal anisotropy (Babuska and Cara, 1991) and is thought to be an important contributor to lower crustal seismic anisotropy (Kitamura, 2006; Tatham et al., 2008). If amphibole LPO behaves similarly at lithospheric mantle depths, in places where the emplacement or subsequent deformation of amphibole has produced an LPO, it is possible that a resulting anisotropic layer modifies the velocity decrease.

6. Discussion and conclusions

Two broad conclusions can be drawn from the above analysis. The first is that partial melt, GBS and changes in Mg# are unlikely to produce large velocity decreases at mid-lithospheric depths within stable continental lithosphere. Unless the aqueous-fluid saturated solidus of Till et al. (2012) proves to be globally applicable, MLD observations are too shallow and therefore cold to feasibly be caused by partial melt, even with unusually fertile or carbon-rich compositions. In any case, there is no obvious reason why migrating melt should consistently accumulate to reach significant porosities in a zone from 80 to 100 km depth in cratonic upper mantle. The velocity decrease associated with GBS is too small and gradual to produce the large MLD phase based on current experimental results. Similarly, velocity reductions associated with Mg# observed in xenolith sections are too small to produce the MLD and generally occur at greater depths within the lithosphere.

The second conclusion is that layers of low-velocity minerals (primarily amphibole) and changes in the geometry of seismic anisotropy are both mechanisms that could feasibly cause velocity reductions of sufficient magnitude to cause the MLD. Of all the mechanisms that have been investigated, a layer of amphibole appears the most likely to be a universal MLD explanation. Most reactions between mantle rocks and ascending fluid or melt will crystallise amphibole at a pressure of ~3 GPa over a broad temperature and compositional range. This could explain the relatively consistent depth of the MLD and provide an explanation for the consistent depth of this feature in both tectonically active and stable continental regions. The challenge for this mechanism is the requirement that all continental lithosphere has undergone sufficient metasomatism to produce a ubiquitous layer rich in amphibole. Mantle xenoliths are an inherently incomplete sample set but the lack of amphibole-rich mantle xenoliths from the Siberian Craton and most of the Slave Craton does raise doubts about the universal presence of an amphibole-rich layer in the continents.

Azimuthal anisotropy will only produce negative SRF conversions in specific geometries and cannot be a universal explanation for the MLD. Radial anisotropy has a more realistic theoretical basis to produce consistent SRF conversions and further research into the specific conversions produced by different geometries would be valuable. However, radial and azimuthal anisotropy in the continents are spatially heterogeneous and varies with tectonic region. Since tectonic histories vary regionally, it is difficult to conceive of a geological process that would induce the same pattern of radial anisotropy in every craton.

It appears likely that there is not one universal cause of the MLD. This assertion is backed up by the SRF data themselves, particularly as data quality and spatial density improve. Since phase conversions are frequency-dependent, different signal frequencies and filtering produce different SRF responses. Longer periods of signal and/or filter band-width can result in interference between phases from adjacent conversions, producing an apparently larger and more continuous phase than actually exists. Chen (2009) shows that a synthetic feature that appears laterally continuous when bandpass filtered at 4–33 s has a smaller amplitude, is laterally discontinuous and sometimes separates vertically into several discrete features when filtered at 2.5–33 s. The laterally discontinuous nature of some MLD phases is demonstrated in a spatially dense SRF network in South Africa (Sodoudi et al., 2013) where an interpreted shallow (~80 km) MLD passes through regions of positive as well as negative SRF phases and a deeper interpreted MLD moves between ~140 km and ~190 km depth to track dominantly negative SRF phases. Foster et al. (2014) analyse similarly spatially dense data from the north-western USA and even with very long-period (8–33 s) filtering some lateral discontinuities and multiple positive and negative phases with depth are apparent.

Individual SRF traces also show that there is significantly more complexity in the lithospheric mantle than one simple velocity drop (Fig. 3). Most authors interpret the largest negative SRF phase beneath the Moho as the MLD and it is this feature that has attracted such attention over the past few years. However, this has perhaps masked a broader outcome of SRF observations, which is that lithospheric mantle sections are seismically complex and generally contain numerous positive and negative velocity discontinuities.

The complexity of SRF data beyond a simple, universal negative phase at a homogeneous depth is consistent with our analysis of the potential mechanisms for causing the MLD. We have shown that hydrous minerals and changes in anisotropy are capable of producing significant velocity reductions in the lithospheric mantle but are unlikely to occur ubiquitously. In addition, partial melt may exist in some locations within the lithosphere. Therefore, it seems unlikely that any of these mechanisms act universally and homogeneously throughout the lithospheric mantle. Instead, we suggest that these features occur heterogeneously in continental lithospheric mantle and produce numerous velocity discontinuities. The apparent existence of a larger magnitude velocity drop between ~80 and 100 km is likely partly due to amphibole and partly due to the effects of long-period seismic signals and band-width filtering.

Appendix A. Supplementary material

Supplementary material related to this article can be found online at http://dx.doi.org/10.1016/j.epsl.2014.12.029.

References

Abt, D.L., Fischer, K.M., French, S.W., Ford, H.A., Yuan, H., Romanowicz, B., 2010. North American lithospheric discontinuity structure imaged by Ps and Sp receiver functions. J. Geophys. Res., Solid Earth (1978–2012) 115.

Adam, J.M.-C., Lebedev, S., 2012. Azimuthal anisotropy beneath southern Africa from very broad-band surface-wave dispersion measurements. Geophys. J. Int. 191, 155–174.

Artemieva, I.M., 2009. The continental lithosphere: reconciling thermal, seismic, and petrologic data. Lithos 109, 23–46.

Artemieva, I.M., Mooney, W.D., 2001. Thermal thickness and evolution of Precambrian lithosphere: a global study. J. Geophys. Res., Solid Earth (1978–2012) 106, 16387–16414.

Aulbach, S., Pearson, N.J., O'Reilly, S.Y., Doyle, B.J., 2007. Origins of xenolithic eclogites and pyroxenites from the Central Slave Craton, Canada. J. Petrol. 48, 1843–1873.

Ave Lallemant, H., Mercier, J., Carter, N., Ross, J., 1980. Rheology of the upper mantle: inferences from peridotite xenoliths. Tectonophysics 70, 85–113.

Ayers, J.C., Dittmer, S.K., Layne, G.D., 1997. Partitioning of elements between peridotite and H_2O at 2.0–3.0 GPa and 900–1100 °C, and application to models of subduction zone processes. Earth Planet. Sci. Lett. 150, 381–398.

Babuska, V., Cara, M., 1991. Seismic Anisotropy in the Earth. Springer.

Best, M., 1970. Kaersutite–peridotite inclusions and kindred megacrysts in basanitic lavas, Grand Canyon, Arizona. Contrib. Mineral. Petrol. 27, 25–44.

Best, M., 1974a. Amphibole-bearing cumulate inclusions, Grand Canyon, Arizona and their bearing on silica-undersaturated hydrous magmas in the upper mantle. J. Petrol. 16, 212–236.

Best, M., 1974b. Mantle-derived amphibole within inclusions in alkalic–basaltic lavas. J. Geophys. Res. 79, 2107–2113.

Bostock, M., 1998. Mantle stratigraphy and evolution of the Slave province. J. Geophys. Res., Solid Earth (1978–2012) 103, 21183–21200.

Bostock, M., 1999. Seismic imaging of lithospheric discontinuities and continental evolution. Dev. Geotecton. 24, 1–16.

Bourguinon, S., 2009. Lithospheric deformation at the South Island oblique collision, New Zealand. Victoria University of Wellington, New Zealand. 303 pp.

Boyd, F., Pokhilenko, N., Pearson, D., Mertzman, S., Sobolev, N., Finger, L., 1997. Composition of the Siberian cratonic mantle: evidence from Udachnaya peridotite xenoliths. Contrib. Mineral. Petrol. 128, 228–246.

Carbno, G., Canil, D., 2002. Mantle structure beneath the SW Slave craton, Canada: constraints from garnet geochemistry in the Drybones Bay kimberlite. J. Petrol. 43, 129–142.

Carlson, R.W., Pearson, D.G., James, D.E., 2005. Physical, chemical, and chronological characteristics of continental mantle. Rev. Geophys. 43, 24.

Chen, L., 2009. Lithospheric structure variations between the eastern and central North China Craton from S- and P-receiver function migration. Phys. Earth Planet. Inter. 173, 216–227.

Chen, L., 2010. Concordant structural variations from the surface to the base of the upper mantle in the North China Craton and its tectonic implications. Lithos 120, 96–115.

Chesley, J.T., Rudnick, R.L., Lee, C.-T., 1999. Re–Os systematics of mantle xenoliths from the East African Rift: age, structure, and history of the Tanzanian craton. Geochim. Cosmochim. Acta 63, 1203–1217.

Connolly, J., Kerrick, D., 2002. Metamorphic controls on seismic velocity of subducted oceanic crust at 100–250 km depth. Earth Planet. Sci. Lett. 204, 61–74.

Crampin, S., 1984. An introduction to wave propagation in anisotropic media. Geophys. J. Int. 76, 17–28.

Dasgupta, R., 2013. Ingassing, storage, and outgassing of terrestrial carbon through geologic time. Rev. Mineral. Geochem. 75, 183–229.

Dasgupta, R., Hirschmann, M.M., 2010. The deep carbon cycle and melting in Earth's interior. Earth Planet. Sci. Lett. 298, 1–13.

Debayle, E., Kennett, B., 2000. Anisotropy in the Australasian upper mantle from Love and Rayleigh waveform inversion. Earth Planet. Sci. Lett. 184, 339–351.

Dick, H., 1989. Abyssal peridotites, very slow spreading ridges and ocean ridge magmatism. In: Geological Society, London, Special Publications, vol. 42, pp. 71–105.

Downes, P.J., Griffin, B.J., Griffin, W.L., 2007. Mineral chemistry and zircon geochronology of xenocrysts and altered mantle and crustal xenoliths from the Aries micaceous kimberlite: constraints on the composition and age of the central Kimberley Craton, Western Australia. Lithos 93, 175–198.

Edwards, D., Rock, N., Taylor, W., Griffin, B., Ramsay, R., 1992. Mineralogy and petrology of the Aries diamondiferous kimberlite pipe, central Kimberley block, Western Australia. J. Petrol. 33, 1157–1191.

Farra, V., Vinnik, L., 2000. Upper mantle stratification by P and S receiver functions. Geophys. J. Int. 141, 699–712.

Faul, U.H., Jackson, I., 2005. The seismological signature of temperature and grain size variations in the upper mantle. Earth Planet. Sci. Lett. 234, 119–134.

Ferguson, J., Sheraton, J., 1979. Petrogenesis of kimberlitic rocks and associated xenoliths of southeastern Australia. In: Kimberlites, Diatremes, and Diamonds: Their Geology, Petrology, and Geochemistry, pp. 140–160.

Fichtner, A., Kennett, B.L., Igel, H., Bunge, H.-P., 2010. Full waveform tomography for radially anisotropic structure: new insights into present and past states of the Australasian upper mantle. Earth Planet. Sci. Lett. 290, 270–280.

Ford, H., 2013. A seismological perspective on the lithosphere–asthenosphere boundary. Brown University. 172 pp.

Ford, H.A., Fischer, K.M., Abt, D.L., Rychert, C.A., Elkins-Tanton, L.T., 2010. The lithosphere–asthenosphere boundary and cratonic lithospheric layering beneath Australia from Sp wave imaging. Earth Planet. Sci. Lett. 300, 299–310.

Foster, K., Dueker, K., Schmandt, B., Yuan, H., 2014. A sharp cratonic lithosphere–asthenosphere boundary beneath the American Midwest and its relation to mantle flow. Earth Planet. Sci. Lett. 402, 82–89.

Fouch, M.J., Rondenay, S., 2006. Seismic anisotropy beneath stable continental interiors. Phys. Earth Planet. Inter. 158, 292–320.

Frederiksen, A., Bostock, M., 2000. Modelling teleseismic waves in dipping anisotropic structures. Geophys. J. Int. 141, 401–412.

Frost, D.J., 2006. The stability of hydrous mantle phases. Rev. Mineral. Geochem. 62, 243–271.

Graham, S., Lambert, D.D., Shee, S.R., Smith, C.B., Reeves, S., 1999. Re–Os isotopic evidence for Archean lithospheric mantle beneath the Kimberley block, Western Australia. Geology 27, 431–434.

Green, D.H., Hibberson, W.O., Kovács, I., Rosenthal, A., 2010. Water and its influence on the lithosphere–asthenosphere boundary. Nature 467, 448–451.

Griffin, W., O'Reilly, S., 1986. The lower crust in eastern Australia: xenolith evidence. In: Geological Society, London, Special Publications, vol. 24, pp. 363–374.

Griffin, W., Wass, S., Hollis, J., 1984. Ultramafic xenoliths from Bullenmerri and Gnotuk maars, Victoria, Australia: petrology of a sub-continental crust–mantle transition. J. Petrol. 25, 53–87.

Griffin, W., Doyle, B., Ryan, C., Pearson, N., Suzanne, Y.R., Davies, R., Kivi, K., Van Achterbergh, E., Natapov, L., 1999. Layered mantle lithosphere in the Lac de Gras area, Slave craton: composition, structure and origin. J. Petrol. 40, 705–727.

Griffin, W., O'Reilly, S.Y., Doyle, B., Pearson, N., Coopersmith, H., Kivi, K., Malkovets, V., Pokhilenko, N., 2004. Lithosphere mapping beneath the North American plate. Lithos 77, 873–922.

Griffin, W., O'Reilly, S.Y., Afonso, J.C., Begg, G., 2009. The composition and evolution of lithospheric mantle: a re-evaluation and its tectonic implications. J. Petrol. 50, 1185–1204.

Hacker, B.R., Abers, G.A., 2004. Subduction factory 3: an Excel worksheet and macro for calculating the densities, seismic wave speeds, and H_2O contents of minerals and rocks at pressure and temperature. Geochem. Geophys. Geosyst. 5.

Hacker, B.R., Abers, G.A., Peacock, S.M., 2003. Subduction factory 1. Theoretical mineralogy, densities, seismic wave speeds, and H_2O contents. J. Geophys. Res., Solid Earth (1978–2012) 108.

Hammond, W.C., Humphreys, E.D., 2000. Upper mantle seismic wave velocity: effects of realistic partial melt geometries. J. Geophys. Res., Solid Earth (1978–2012) 105, 10975–10986.

Handler, M., Bennett, V., Carlson, R., 2005. Nd, Sr and Os isotope systematics in young, fertile spinel peridotite xenoliths from northern Queensland, Australia: a unique view of depleted MORB mantle? Geochim. Cosmochim. Acta 69, 5747–5763.

Hansen, S.E., Nyblade, A.A., Julia, J., Dirks, P.H., Durrheim, R.J., 2009. Upper-mantle low-velocity zone structure beneath the Kaapvaal craton from S-wave receiver functions. Geophys. J. Int. 178, 1021–1027.

Hawkesworth, C., Kempton, P., Rogers, N., Ellam, R., Van Calsteren, P., 1990. Continental mantle lithosphere, and shallow level enrichment processes in the Earth's mantle. Earth Planet. Sci. Lett. 96, 256–268.

Heit, B., Sodoudi, F., Yuan, X., Bianchi, M., Kind, R., 2007. An S receiver function analysis of the lithospheric structure in South America. Geophys. Res. Lett. 34.

Hirschmann, M.M., 2006. Water, melting, and the deep Earth H_2O cycle. Annu. Rev. Earth Planet. Sci. 34, 629–653.

Hughes, D.S., Cross, J.H., 1951. Elastic wave velocities in rocks at high pressures and temperatures. Geophysics 16, 577–593.

Ionov, D.A., Shirey, S.B., Weis, D., Brügmann, G., 2006. Os–Hf–Sr–Nd isotope and PGE systematics of spinel peridotite xenoliths from Tok, SE Siberian craton: effects of pervasive metasomatism in shallow refractory mantle. Earth Planet. Sci. Lett. 241, 47–64.

Jackson, I., Faul, U.H., 2010. Grainsize-sensitive viscoelastic relaxation in olivine: towards a robust laboratory-based model for seismological application. Phys. Earth Planet. Inter. 183, 151–163.

Jackson, I., Faul, U.H., Skelton, R., 2014. Elastically accommodated grain-boundary sliding: new insights from experiment and modeling. Phys. Earth Planet. Inter. 228, 203–210.

Jaupart, C., Mareschal, J.-C., 2011. Heat Generation and Transport in the Earth. Cambridge University Press, Cambridge, UK.

Jordan, T.H., 1978. Composition and development of the continental tectosphere. Nature 274, 544–548.

Jordan, T.H., 1988. Structure and formation of the continental tectosphere. J. Petrol., 11–37.

Julià, J., 2007. Constraining velocity and density contrasts across the crust–mantle boundary with receiver function amplitudes. Geophys. J. Int. 171, 286–301.

Jung, H., Katayama, I., Jiang, Z., Hiraga, T., Karato, S.-I., 2006. Effect of water and stress on the lattice-preferred orientation of olivine. Tectonophysics 421, 1–22.

Karato, S.-i., 2012. On the origin of the asthenosphere. Earth Planet. Sci. Lett. 321, 95–103.

Karato, S.-i., Jung, H., Katayama, I., Skemer, P., 2008. Geodynamic significance of seismic anisotropy of the upper mantle: new insights from laboratory studies. Annu. Rev. Earth Planet. Sci. 36, 59–95.

Keith, C.M., Crampin, S., 1977. Seismic body waves in anisotropic media: reflection and refraction at a plane interface. Geophys. J. Int. 49, 181–208.

Kelemen, P.B., Hart, S.R., Bernstein, S., 1998. Silica enrichment in the continental upper mantle via melt/rock reaction. Earth Planet. Sci. Lett. 164, 387–406.

Kind, R., Yuan, X., Kumar, P., 2012. Seismic receiver functions and the lithosphere–asthenosphere boundary. Tectonophysics 536, 25–43.

Kind, R., Sodoudi, F., Yuan, X., Shomali, H., Roberts, R., Gee, D., Eken, T., Bianchi, M., Tilmann, F., Balling, N., 2013. Scandinavia: a former Tibet? Geochem. Geophys. Geosyst. 14, 4479–4487.

Kitamura, K., 2006. Constraint of lattice-preferred orientation (LPO) on Vp anisotropy of amphibole-rich rocks. Geophys. J. Int. 165, 1058–1065.

Konzett, J., Armstrong, R.A., Günther, D., 2000. Modal metasomatism in the Kaapvaal craton lithosphere: constraints on timing and genesis from U–Pb zircon dating of metasomatized peridotites and MARID-type xenoliths. Contrib. Mineral. Petrol. 139, 704–719.

Konzett, J., Wirth, R., Hauzenberger, C., Whitehouse, M., 2013. Two episodes of fluid migration in the Kaapvaal Craton lithospheric mantle associated with Cretaceous kimberlite activity: evidence from a harzburgite containing a unique assemblage of metasomatic zirconium-phases. Lithos 182, 165–184.

Kopylova, M., Caro, G., 2004. Mantle xenoliths from the southeastern Slave craton: evidence for chemical zonation in a thick, cold lithosphere. J. Petrol. 45, 1045–1067.

Kopylova, M.G., Russell, J.K., 2000. Chemical stratification of cratonic lithosphere: constraints from the Northern Slave craton, Canada. Earth Planet. Sci. Lett. 181, 71–87.

Kopylova, M., Russell, J., Cookenboo, H., 1999. Petrology of peridotite and pyroxenite xenoliths from the Jericho kimberlite: implications for the thermal state of the mantle beneath the Slave craton, northern Canada. J. Petrol. 40, 79–104.

Kumar, P., Kind, R., Yuan, X., Mechie, J., 2012. USArray receiver function images of the lithosphere–asthenosphere boundary. Seismol. Res. Lett. 83, 486–491.

Kumar, P., Ravi Kumar, M., Srijayanthi, G., Arora, K., Srinagesh, D., Chadha, R., Sen, M.K., 2013. Imaging the lithosphere–asthenosphere boundary of the Indian plate using converted wave techniques. J. Geophys. Res., Solid Earth 118, 5307–5319.

Langston, C.A., 1979. Structure under Mount Rainier, Washington, inferred from teleseismic body waves. J. Geophys. Res., Solid Earth (1978–2012) 84, 4749–4762.

Lebedev, S., Boonen, J., Trampert, J., 2009. Seismic structure of Precambrian lithosphere: new constraints from broad-band surface-wave dispersion. Lithos 109, 96–111.

Lee, C.-T.A., 2006. Geochemical/petrologic constraints on the origin of cratonic mantle. In: Archean Geodynamics and Environments, vol. 164, pp. 89–114.

Lee, L., Morris, S., 2010. Anelasticity and grain boundary sliding. Proc. R. Soc., Math. Phys. Eng. Sci. 466, 2651–2671.

Lekić, V., Fischer, K.M., 2014. Contrasting lithospheric signatures across the western United States revealed by Sp receiver functions. Earth Planet. Sci. Lett. 402, 90–98.

Levin, V., Park, J., 1997. P–SH conversions in a flat-layered medium with anisotropy of arbitrary orientation. Geophys. J. Int. 131, 253–266.

Levin, V., Park, J., 2000. Shear zones in the Proterozoic lithosphere of the Arabian Shield and the nature of the Hales discontinuity. Tectonophysics 323, 131–148.

Li, C., van der Hilst, R.D., Engdahl, E.R., Burdick, S., 2008. A new global model for P wave speed variations in Earth's mantle. Geochem. Geophys. Geosyst. 9.

Luguet, A., Jaques, A., Pearson, D., Smith, C., Bulanova, G., Roffey, S., Rayner, M., Lorand, J.-P., 2009. An integrated petrological, geochemical and Re–Os isotope study of peridotite xenoliths from the Argyle lamproite, Western Australia and implications for cratonic diamond occurrences. Lithos 112, 1096–1108.

Marone, F., Gung, Y., Romanowicz, B., 2007. Three-dimensional radial anisotropic structure of the North American upper mantle from inversion of surface waveform data. Geophys. J. Int. 171, 206–222.

Mercier, J.-P., Bostock, M., Audet, P., Gaherty, J., Garnero, E., Revenaugh, J., 2008. The teleseismic signature of fossil subduction: northwestern Canada. J. Geophys. Res., Solid Earth (1978–2012) 113.

Meyer, H.O., Waldman, M., Garwood, B., 1994. Mantle xenoliths from kimberlite near Kirkland Lake, Ontario. Can. Mineral. 32, 295.

Miller, M.S., Eaton, D.W., 2010. Formation of cratonic mantle keels by arc accretion: evidence from S receiver functions. Geophys. Res. Lett. 37.

Moorkamp, M., Jones, A., Fishwick, S., 2010. Joint inversion of receiver functions, surface wave dispersion, and magnetotelluric data. J. Geophys. Res., Solid Earth (1978–2012) 115.

Morris, S., Jackson, I., 2009. Diffusionally assisted grain-boundary sliding and viscoelasticity of polycrystals. J. Mech. Phys. Solids 57, 744–761.

Nettles, M., Dziewoński, A.M., 2008. Radially anisotropic shear velocity structure of the upper mantle globally and beneath North America. J. Geophys. Res., Solid Earth (1978–2012) 113.

Ni, H., Keppler, H., Behrens, H., 2011. Electrical conductivity of hydrous basaltic melts: implications for partial melting in the upper mantle. Contrib. Mineral. Petrol. 162, 637–650.

Nyblade, A.A., Pollack, H.N., 1993. A global analysis of heat flow from Precambrian terrains: implications for the thermal structure of Archean and Proterozoic lithosphere. J. Geophys. Res., Solid Earth (1978–2012) 98, 12207–12218.

O'Reilly, S., Griffin, W., 1985. A xenolith-derived geotherm for southeastern Australia and its geophysical implications. Tectonophysics 111, 41–63.

Olugboji, T., Karato, S., Park, J., 2013. Structures of the oceanic lithosphere–asthenosphere boundary: mineral-physics modeling and seismological signatures. Geochem. Geophys. Geosyst. 14, 880–901.

Pearson, D., Shirey, S., Carlson, R., Boyd, F.R., Pokhilenko, N., Shimizu, N., 1995. Re–Os, Sm–Nd, and Rb–Sr isotope evidence for thick Archaean lithospheric mantle beneath the Siberian craton modified by multistage metasomatism. Geochim. Cosmochim. Acta 59, 959–977.

Powell, W., Zhang, M., O'Reilly, S.Y., Tiepolo, M., 2004. Mantle amphibole trace-element and isotopic signatures trace multiple metasomatic episodes in lithospheric mantle, western Victoria, Australia. Lithos 75, 141–171.

Priestley, K., McKenzie, D., 2006. The thermal structure of the lithosphere from shear wave velocities. Earth Planet. Sci. Lett. 244, 285–301.

Raj, R., Ashby, M., 1971. On grain boundary sliding and diffusional creep. Metall. Trans. 2, 1113–1127.

Richardson, S., Shirey, S., Harris, J., Carlson, R., 2001. Archean subduction recorded by Re–Os isotopes in eclogitic sulfide inclusions in Kimberley diamonds. Earth Planet. Sci. Lett. 191, 257–266.

Ringwood, A., 1966. Chemical evolution of the terrestrial planets. Geochim. Cosmochim. Acta 30, 41–104.

Rudnick, R.L., McDonough, W.F., O'Connell, R.J., 1998. Thermal structure, thickness and composition of continental lithosphere. Chem. Geol. 145, 395–411.

Rychert, C.A., Shearer, P.M., 2009. A global view of the lithosphere–asthenosphere boundary. Science 324, 495–498.

Rychert, C.A., Rondenay, S., Fischer, K.M., 2007. P-to-S and S-to-P imaging of a sharp lithosphere–asthenosphere boundary beneath eastern North America. J. Geophys. Res., Solid Earth (1978–2012) 112.

Saltzer, R.L., 2002. Upper mantle structure of the Kaapvaal craton from surface wave analysis—a second look. Geophys. Res. Lett. 29. 11-11–11-14.

Saul, J., Kumar, M.R., Sarkar, D., 2000. Lithospheric and upper mantle structure of the Indian Shield, from teleseismic receiver functions. Geophys. Res. Lett. 27, 2357–2360.

Savage, B., Silver, P.G., 2008. Evidence for a compositional boundary within the lithospheric mantle beneath the Kalahari craton from S receiver functions. Earth Planet. Sci. Lett. 272, 600–609.

Savage, M.K., 1998. Lower crustal anisotropy or dipping boundaries? Effects on receiver functions and a case study in New Zealand. J. Geophys. Res., Solid Earth (1978–2012) 103, 15069–15087.

Schaeffer, A., Lebedev, S., 2013. Global shear speed structure of the upper mantle and transition zone. Geophys. J. Int. 194, 417–449. ggt095.

Schutt, D., Lesher, C., 2006. Effects of melt depletion on the density and seismic velocity of garnet and spinel lherzolite. J. Geophys. Res., Solid Earth (1978–2012) 111.

Sebai, A., Stutzmann, E., Montagner, J.-P., Sicilia, D., Beucler, E., 2006. Anisotropic structure of the African upper mantle from Rayleigh and Love wave tomography. Phys. Earth Planet. Inter. 155, 48–62.

Selway, K., 2014. On the causes of electrical conductivity anomalies in tectonically stable lithosphere. Surv. Geophys. 35, 219–257.

Sifré, D., Gardés, E., Massuyeau, M., Hashim, L., Hier-Majumder, S., Gaillard, F., 2014. Electrical conductivity during incipient melting in the oceanic low-velocity zone. Nature 509, 81–85.

Silver, P.G., 1996. Seismic anisotropy beneath the continents: probing the depths of geology. Annu. Rev. Earth Planet. Sci. 24, 385–432.

Simons, F.J., van der Hilst, R.D., 2002. Age-dependent seismic thickness and mechanical strength of the Australian lithosphere. Geophys. Res. Lett. 29, 1529.

Simons, F.J., van der Hilst, R.D., 2003. Seismic and mechanical anisotropy and the past and present deformation of the Australian lithosphere. Earth Planet. Sci. Lett. 211, 271–286.

Snyder, D.B., 2008. Stacked uppermost mantle layers within the Slave craton of NW Canada as defined by anisotropic seismic discontinuities. Tectonics 27.

Sodoudi, F., Yuan, X., Kind, R., Lebedev, S., Adam, J.M.C., Kästle, E., Tilmann, F., 2013. Seismic evidence for stratification in composition and anisotropic fabric within the thick lithosphere of Kalahari Craton. Geochem. Geophys. Geosyst. 14, 5393–5412.

Sundberg, M., Cooper, R.F., 2010. A composite viscoelastic model for incorporating grain boundary sliding and transient diffusion creep; correlating creep and attenuation responses for materials with a fine grain size. Philos. Mag. 90, 2817–2840.

Sweeney, R., Thompson, A., Ulmer, P., 1993. Phase relations of a natural MARID composition and implications for MARID genesis, lithospheric melting and mantle metasomatism. Contrib. Mineral. Petrol. 115, 225–241.

Tappe, S., Foley, S.F., Kjarsgaard, B.A., Romer, R.L., Heaman, L.M., Stracke, A., Jenner, G.A., 2008. Between carbonatite and lamproite—diamondiferous Torngat ultramafic lamprophyres formed by carbonate-fluxed melting of cratonic MARID-type metasomes. Geochim. Cosmochim. Acta 72, 3258–3286.

Tatham, D., Lloyd, G., Butler, R., Casey, M., 2008. Amphibole and lower crustal seismic properties. Earth Planet. Sci. Lett. 267, 118–128.

Thybo, H., 2006. The heterogeneous upper mantle low velocity zone. Tectonophysics 416, 53–79.

Thybo, H., Perchuć, E., 1997. The seismic 8 discontinuity and partial melting in continental mantle. Science 275, 1626–1629.

Till, C.B., Grove, T.L., Withers, A.C., 2012. The beginnings of hydrous mantle wedge melting. Contrib. Mineral. Petrol. 163, 669–688.

van Achterbergh, E., Griffin, W.L., Stiefenhofer, J., 2001. Metasomatism in mantle xenoliths from the Letlhakane kimberlites: estimation of element fluxes. Contrib. Mineral. Petrol. 141, 397–414.

Vicker, P.A., 1997. Garnet peridotite xenoliths from kimberlite near Kirkland Lake, Canada. University of Toronto.

Wass, S.Y., Rogers, N., 1980. Mantle metasomatism—precursor to continental alkaline volcanism. Geochim. Cosmochim. Acta 44, 1811–1823.

Waters, F., Erlank, A., 1988. Assessment of the vertical extent and distribution of mantle metasomatism below Kimberley, South Africa. J. Petrol., 185–204.

Wilshire, H., Pike, J.N., Meyer, C., Schwarzman, E., 1980. Amphibole-rich veins in lherzolite xenoliths, Dish Hill and Deadman Lake, California. Am. J. Sci. A 280, 576–593.

Wirth, E.A., Long, M.D., 2014. A contrast in anisotropy across mid-lithospheric discontinuities beneath the central United States – a relic of craton formation. Geology 42, 851–854.

Wittlinger, G., Farra, V., 2007. Converted waves reveal a thick and layered tectosphere beneath the Kalahari super-craton. Earth Planet. Sci. Lett. 254, 404–415.

Wölbern, I., Rümpker, G., Link, K., Sodoudi, F., 2012. Melt infiltration of the lower lithosphere beneath the Tanzania craton and the Albertine rift inferred from S receiver functions. Geochem. Geophys. Geosyst. 13.

Wyllie, P.J., 1987. Discussion of recent papers on carbonated peridotite, bearing on mantle metasomatism and magmatism. Earth Planet. Sci. Lett. 82, 391–397.

Yuan, H., Romanowicz, B., 2010. Lithospheric layering in the North American craton. Nature 466, 1063–1068.

Yuan, H., Romanowicz, B., Fischer, K.M., Abt, D., 2011. 3-D shear wave radially and azimuthally anisotropic velocity model of the North American upper mantle. Geophys. J. Int. 184, 1237–1260.

Yuan, X., Kind, R., Li, X., Wang, R., 2006. The S receiver functions: synthetics and data example. Geophys. J. Int. 165, 555–564.

Zhou, L., Chen, W.-P., Özalaybey, S., 2000. Seismic properties of the central Indian shield. Bull. Seismol. Soc. Am. 90, 1295–1304.

Kate Selway is currently working as a research scientist at Lamont–Doherty Earth Observatory, where she has been since 2013. Kate received her Ph.D. from the University of Adelaide, South Australia, in 2007. Her main interest is in combining geophysical data, particularly MT, with geological, geochemical and mineral physics data to improve our understanding of continental composition and evolution.

Heather A. Ford is currently a postdoctoral associate in the Geology and Geophysics Department at Yale University, where she has been since 2013. Heather received her Ph.D. from Brown University, in 2013 and her M.Sc., in 2009. Heather completed her undergraduate education at the University of Michigan, in 2005, receiving a B.S. in Geological Sciences.

Peter Kelemen is the Arthur D. Storke Memorial Professor of geochemistry at Lamont–Doherty Earth Observatory and chair of Earth and Environmental Sciences at Columbia University. Peter's research interests include CO_2 capture and storage via in situ mineral carbonation in peridotite and basalt, melting and reactive melt transport in the Earth's mantle and lower crust, igneous processes in forming the Earth's crust, density instabilities, ductile deformation and evolution of the lower crust, subduction zone geotherms and the mechanisms for intermediate depth earthquakes